ADVANCED MATERIALS
www.advmat.de

Dual-Targeted Lipid Nanotherapeutic Boost for Chemo-Immunotherapy of Cancer

*Seok-Beom Yong, Srinivas Ramishetti, Meir Goldsmith, Yael Diesendruck, Inbal Hazan-Halevy, Sushmita Chatterjee, Gonna Somu Naidu, Assaf Ezra, and Dan Peer**

Chemo-immunotherapy is a combination of "standard-of-care" chemotherapy with immunotherapy and it is considered the most advanced therapeutic modality for various types of cancers. However, many cancer patients still poorly respond to current regimen of chemo-immunotherapy and suggest nanotherapeutics as a boosting agent. Recently, heme oxygenase-1 (HO1) is shown to act as an immunotherapeutic molecule in tumor myeloid cells, in addition to general chemoresistance function in cancer cells suggesting that HO1-targeted therapeutics can become a novel, optimal strategy for boosting chemo-immunotherapy in the clinic. Currently the available HO1-inhibitors demonstrate serious adverse effects in clinical use. Herein, tumor myeloid cell- and cancer cell-dual targeted HO1-inhibiting lipid nanotherapeutic boost (T-iLNTB) is developed using RNAi-loaded lipid nanoparticles. T-iLNTB-mediated HO1-inhibition sensitizes cancer cells to "standard-of-care" chemotherapeutics by increasing immunogenic cell death, and directly reprograms tumor myeloid cells with distinguished phenotype. Furthermore, tumor myeloid cell reprogramming by T-iLNTB induces $CD8^+$ cytotoxic T cell recruitment, which drives "Cold-to-Hot" transition and correlates with improved responsiveness to immune checkpoint inhibitor in combination therapy. Finally, ex vivo study proves that HO1-inhibition directly affects tumor macrophage differentiation. This study demonstrates the potential of T-iLNTB as a novel therapeutic modality for boosting chemo-immunotherapy.

1. Introduction

Cancer immunotherapy reinvigorates the suppressed immune system, which induces antitumoral immune responses against malignant cells. Immune checkpoint inhibitors (ICIs), such as anti-PD1 and anti-CTLA4 antibodies, are among the most successful immunotherapy modalities that have shown therapeutic benefits in various types of cancers, from melanoma to lung cancer.[1] However, only a minority of cancer patients are responsive to ICIs therapy, depending on their immunophenotype and cancer genotype.[2] Chemo-immunotherapy is a combination of "standard-of-care" chemotherapy with immunotherapy, mostly ICIs such as nivolumab and pembrolizumab that shows therapeutic benefit in the clinic and success in phase III trials.[3] Yet, many patients are still poorly responsive to this combination therapy and nanotherapeutics could be a novel strategy for the improvement of chemo-immunotherapy.

The tumor immune microenvironment is enriched with various immune cells from myeloid cells to lymphocytes. Tumor myeloid cells including monocytes and macrophages are recruited by the inflamed cancer cell niche and paradoxically induce "immunosuppressive" status in solid tumors.[2b,4] In particular, tumor-associated macrophages (TAM) that are originated from tumor-infiltrated monocytes[5] directly remodel the tumor immune microenvironment by physically impeding infiltration of cytotoxic $CD8^+$ T lymphocytes and

S.-B. Yong, S. Ramishetti, M. Goldsmith, Y. Diesendruck, I. Hazan-Halevy, S. Chatterjee, G. Somu Naidu, A. Ezra, D. Peer
Laboratory of Precision Nanomedicine
The Shmunis School of Biomedicine and Cancer Research
George S. Wise Faculty of Life Sciences
Tel Aviv University
Tel-Aviv 69978, Israel
E-mail: peer@post.tau.ac.il

The ORCID identification number(s) for the author(s) of this article can be found under https://doi.org/10.1002/adma.202106350.

DOI: 10.1002/adma.202106350

S.-B. Yong, S. Ramishetti, M. Goldsmith, Y. Diesendruck, I. Hazan-Halevy, S. Chatterjee, G. Somu Naidu, A. Ezra, D. Peer
Department of Materials Sciences and Engineering
Iby and Aladar Fleischman Faculty of Engineering
Tel Aviv University
Tel Aviv 69978, Israel

S.-B. Yong, S. Ramishetti, M. Goldsmith, Y. Diesendruck, I. Hazan-Halevy, S. Chatterjee, G. Somu Naidu, A. Ezra, D. Peer
Center for Nanoscience and Nanotechnology
Tel Aviv University
Tel Aviv 69978, Israel

S.-B. Yong, S. Ramishetti, M. Goldsmith, Y. Diesendruck, I. Hazan-Halevy, S. Chatterjee, G. Somu Naidu, A. Ezra, D. Peer
Cancer Biology Research Center
Tel Aviv University
Tel Aviv 69978, Israel

promote their exclusion from the tumor microenvironment.[6] This is a major cellular determinant of immunologically "Hot" and "Cold" status of solid tumors, and is correlated with the responsiveness of cancer patients to immunotherapy.[2a] Thus, tumor myeloid cell-targeted therapy is a promising strategy for immunotherapeutic enhancement, especially for the potential transition from "Cold" to "Hot" tumor. Due to its ease of surface modification, the capacity of drug loading, and passive tumor targeting, nanoparticles have been employed for tumor-targeted drug delivery.[4] Recently, various types of nanoparticles have been developed for cancer chemo-immunotherapy combination.[7] However, their preparation includes multiple components and complicated steps that are unrealizable for large-scale production and make them clinically irrelevant. Furthermore, different solubility and release kinetics could be a serious obstacle for clinical-grade preparation of multiple drug-loaded formulations for chemo-immunotherapy.[8] Hence, a simple and practical strategy is required to improve the current chemo-immunotherapy treatments.

Heme oxygenase-1 (HO1) is a stress-inducible, cytoprotective, and antioxidative enzyme, which catalyzes heme degradation into carbon monoxide (CO), biliverdin, and iron. HO1-produced CO is known as a major immunomodulatory, immune suppressive mediator. HO1 has been previously reported to have protumorigenic characteristics,[9] as its induction leads to chemoresistance in various human and mouse cancer cell lines.[10] Moreover, in recent studies HO1 was shown to mediate M1/M2 macrophage polarization in part, and myeloid cell lineage-specific knockout of HO1 induces antitumor immunity through tumor-myeloid reprogramming and cytotoxic T cell activation. This suggests HO1 as a novel immune checkpoint molecule in tumor myeloid cells, as shown both in mouse tumor models and human samples.[11] Collectively, HO1 is a novel therapeutic target and HO1-targeted drug delivery could be a cost-effective and optimal strategy to boost chemo-immunotherapy. A recent study reported a "proof-of-concept" of HO1-targeted nanotherapeutics by using Tin mesoporphyrin (SnMP)-loaded nanoparticles.[12] However, small molecule inhibitors of HO1, such as SnMP and zinc protoporphyrin (ZnPP), have nonspecificity issue with HO2,[13] an isoform of HO1 with more constitutive expression in various tissues including the brain. In addition, ZnPP showed HO1-inhibition independent effect in cellular pathways,[14] and the FDA approval for compassionate use of SnMP in hyper bilirubinemia was terminated and has been rejected for FDA approval since 2018.

RNA-interference (RNAi)-based modalities offer a more specific strategy, preferable to small molecule inhibitors for pharmacological inhibition of HO1. In addition, the previously reported nanoparticle approach is clinically irrelevant due to the obstacles of batch-to-batch variation and large-scale preparation issues.[12] Lipid nanoparticles (LNPs) are the most advanced and clinically approved nonviral delivery of nucleic acid therapeutics as evident by the FDA approval of Patisiran and COVID19 mRNA vaccines. To date several nucleic acid therapeutics based on LNP systems are in clinical trials for human diseases including cancers.[15] Furthermore, microfluidics-based preparation of LNPs yield homogeneous, uniform LNPs suitable for large-scale production, a critical factor for designing clinically relevant cancer-targeted RNAi drug delivery.[16] We previously reported several novel ionizable lipids demonstrating improved nucleic acid delivery compared to the current gold standard lipid, DLin-MC3-DMA, in cancer cells.[17] In addition, we previously described a unique lipoprotein linker system, anchored secondary scFv enabling targeting (ASSET), that facilitates an efficient modification of LNPs with a targeting antibody of choice for in vivo-targeted delivery of LNPs to specific cell population.[18] Here, we entrapped siRNA against HO1 in lipid nanoparticles (ionizable lipid nanotherapeutic boost (iLNTB)) and modified their surface with anti-PD-L1 antibody to generate cancer- and tumor myeloid cell-targeted lipid nanotherapeutic boost (T-iLNTB) for dual effect of chemotherapeutic enhancement ("chemoboost") and immunological reprogramming ("immunoboost") in tumors. Finally, we combined the T-iLNTB with conventional chemotherapy and ICI for chemo- and immunotherapeutic boost of cancer therapy (**Scheme 1**).

2. Results and Discussion

2.1. Physicochemical Characterization of iLNTB

We used an ionizable LNP/RNAi approach, which is the most advanced nonviral RNAi delivery platform for human use and also highly potent for HO1-specific inhibition.[15b] In addition, we incorporated an anti-PD-L1 antibody on the surface of the LNP by using the ASSET system for dual targeting of cancer and tumor myeloid cells (**Figure 1**a).[19] We used a novel ionizable lipid designed in our lab, lipid 8 (see Figure S1a, Supporting Information), that previously showed efficient nucleic acid delivery for siRNA and mRNA.[17,20] LNPs entrapping RNAi were generated using a microfluidic mixing device (see the Experimental Section, Supporting Information). We prepared two different LNPs encapsulating either HO1 siRNA (iLNTB) or nonspecific control siRNA (iLNC). As shown in Figure 1b, our preparation method produced homogeneous LNPs with narrow size distribution of 61.46 ± 8.54 nm for iLNC and 66.66 ± 10.16 nm for iLNTB, and ζ-potential of 3.07 ± 0.95 and 3.5 ± 1.51 mV for iLNC and iLNTB, respectively, as measured by dynamic light scattering (DLS). Next, we evaluated the stability of RNA in the LNPs over time, as undesirable drug release and instability of nanoparticles hamper their clinical translation. The RNA entrapment (% to total RNA in the sample) in iLNTB was determined as 95.85% ± 2.13% 1 day after preparation and mildly decreased to 91.52% ± 2.86% at 30 days postpreparation, demonstrating the stability of the LNPs when stored at 4 °C (Figure 1c). In addition, we observed the encapsulation efficiency (normalized to the original RNA amount used) of 95.69% ± 2.73%. We then coated the LNPs with the lipidated secondary single-chain Fv fragment (ASSET), that binds to the Fc region of Rat IgG2a with dissociation constant (K_d) of ≈22.7×10^{-9} M, and enables noncovalent modification of LNPs with various antibodies for cell type-specific targeting.[18] To optimize the amount of ASSET on the surface of LNPs, three different amounts of ASSET, 2, 4, and 8 μg were incorporate into iLNTB. As shown in Figure 1d, ASSET-incorporation increased the size distribution of LNP from 73.26 nm (ASSET 0 μg) to 95.5 nm (ASSET 2 μg), 93.13 nm (ASSET 4 μg), 88.83 nm (ASSET 8 μg), and decreased ζ-potential of

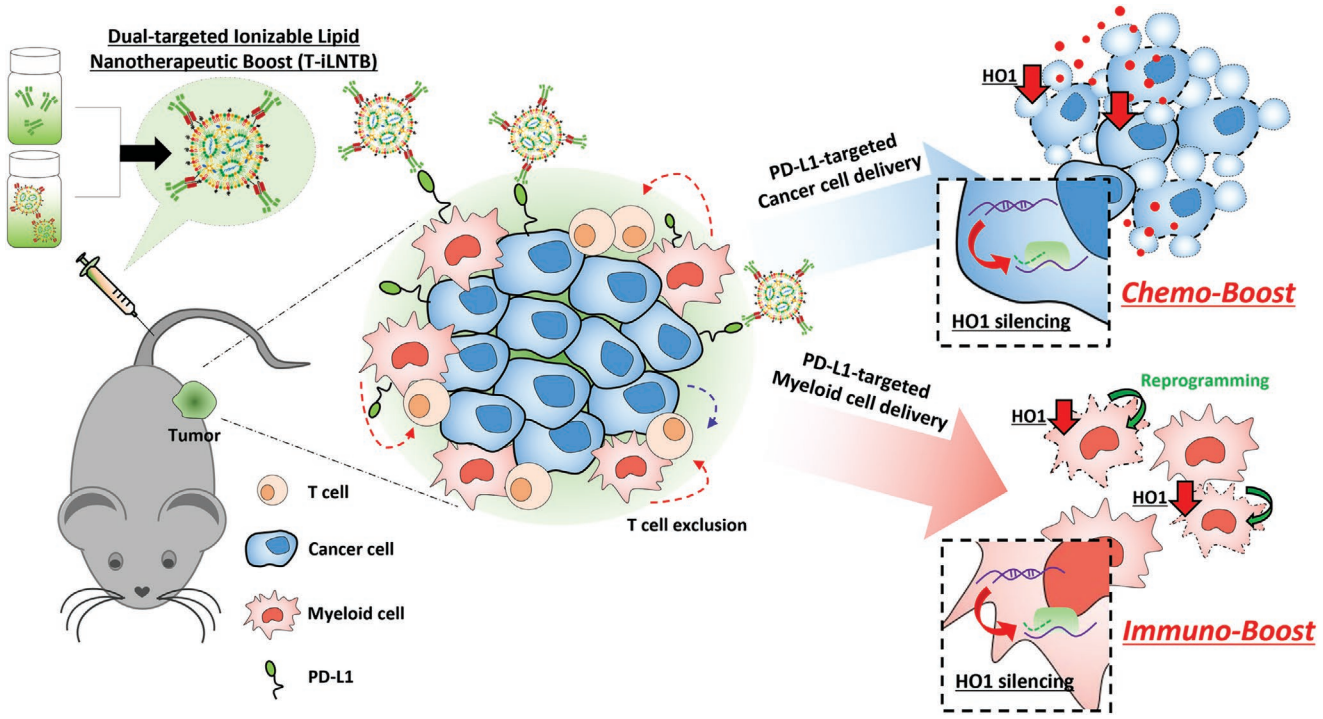

Scheme 1. Schematic diagram of dual-targeted ionizable lipid nanotherapeutic boost (T-iLNTB) for chemo-immunotherapy. T-iLNTB is actively targeted to PD-L1-experssing cells, including cancer cells and tumor-associated myeloid cells. HO1 silencing by T-iLNTB sensitizes cancer cells to chemotherapy for "chemoboosting" and reprograms tumor myeloid cells for "immunoboosting."

LNP to −4.38 mV (ASSET 2 μg), −4.83 mV (ASSET 4 μg), and −9.95 mV (ASSET 8 μg). In addition, polydispersity index (PDI) was increased from ≈0.04 for iLNTB to ≈0.12 for ASSET-incorporated iLNTBs. Upon incorporation of different amounts of ASSET, their size and PDI did not change for a month except the ASSET 8 μg-incorporated iLNTB, which showed an increase in size distribution from 21 days post ASSET incorporation, and therefore, excluded from further experiments (Figure 1e; Figure S1b, Supporting Information). ASSET-incorporated iLNTB showed a slight increase in size distribution measured by transmission electron microscopy, in comparison with iLNTB, which is in agreement with the DLS results (Figure 1f; Figure S1b, Supporting Information).

2.2. In Vitro Chemoboosting Effect of iLNTB in Cancer Cells

An antioxidant and cytoprotective induction of HO1 has been reported to induce a chemoresistance in cancer cells (both in solid tumors and blood cancers[10b,c]). To validate the chemoboosting effect of iLNTB, murine melanoma (B16F10) and murine breast cancer cells (E0771) were treated with iLNTB. Cy5-labeled iLNTB showed a rapid cellular uptake for both type of cells upon 30 min incubation of iLNTB (**Figure 2**a). The iLNTB mostly distributed in the cytosolic and perinuclear compartment. Next, B16F10 and E0771 cells were treated with iLNC and iLNTB in the presence of "standard-of-care" chemotherapy, Doxorubicin (Dox). Dox, an anthracycline drug, is being used for chemo-immunotherapy in the clinic,[3] and is known for inducing immunogenic cell death in cancer cells,[21] which is an important trigger for antitumor immune response in chemo-immuno combination therapy. In addition, Dox has shown strong therapeutic effect in combination with immunotherapy in comparison with other anticancer drugs.[3] In a preliminary experiment, we screened the best HO1 siRNA sequence from three different candidates based on the HO1 gene silencing effect as reflected by the mRNA levels. Candidate 2 was chosen to prepare iLNTB (Figure S2a, Supporting Information). Compared to untreated and iLNC-treated cells, iLNTB treatment significantly decreased HO1 mRNA levels and suppressed Dox-responsive HO1 upregulation (Figure 2b). As expected, HO2 mRNA levels were not reduced by iLNTB treatment (Figure S2b, Supporting Information). The protein levels of HO1 were upregulated in response to Dox and completely suppressed by iLNTB treatment in B16F10 cells (Figure 2c). E0771 cells showed a higher basal level of HO1 protein expression compared to B16F10 cells, which were slightly increased by Dox treatment but completely suppressed by iLNTB treatment. E0771 cells show higher HO1 mRNA level compared to B16F10 which was in agreement with the protein expression (Figure S2c, Supporting Information). The iLNTB-mediated HO1-inhibition in both types of cancer cells increased the sensitivity of cells to Dox in a dose-dependent manner, with decreased cell viability in comparison with control and iLNC group (Figure 2d; Figure S2d, Supporting Information). At the Dox concentration of 0.5×10^{-6} M, B16F10 and E0771 shows 1.47- and 1.6-fold higher responsiveness to Dox in the T-iLNTB group compared to control. Although there is a direct effect of HO1 silencing on cancer cell viability, it is very weak compared to other types of cytotoxic, anticancer agent such as Dox. Compared to Dox, which

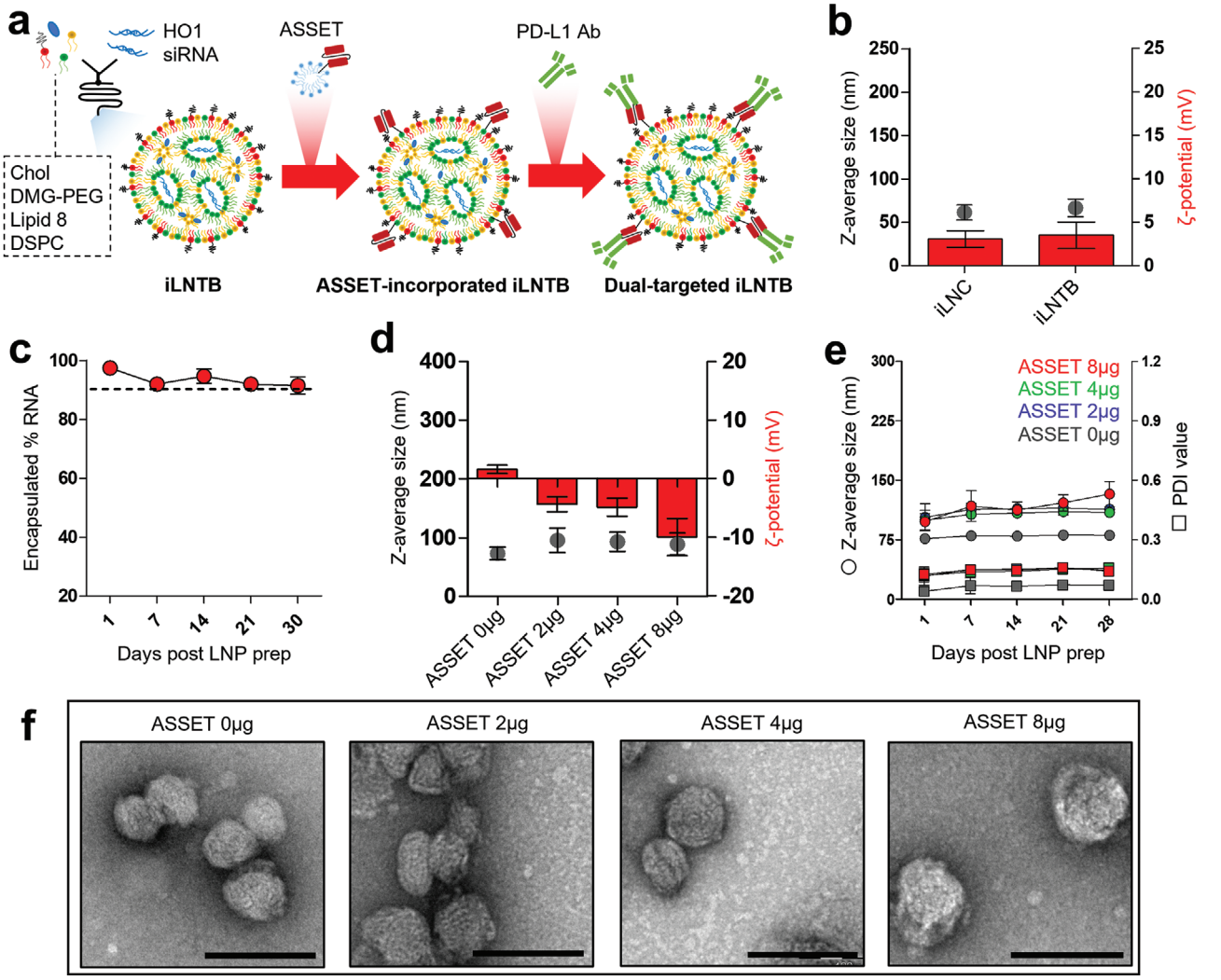

Figure 1. Physicochemical characterization of iLNTB and ASSET incorporation. a) Schematic illustration of microfluidic preparation of iLNTB, ASSET-incorporation, and targeting antibody modification. iLNTB was produced using HO1 siRNA, ionizable lipid 8, and helper-lipids, Chol: Cholesterol. b) Size and ζ-potential measurements of iLNTB and iLNC. c) Stability of RNA encapsulation in iLNTB. iLNTB-encapsulated RNA was quantified by RiboGreen assay and normalized to total RNA. d) DLS analysis of ASSET-incorporated iLNTB. iLNTB was incorporated with various amount of ASSET protein and analyzed for its size and ζ-potential. e) Stability of ASSET-incorporated iLNTB. ASSET-incorporated iLNTB was analyzed by DLS at indicated days after preparation to analyze its nanosize and polydispersity. f) Transmission electron microscopy image of ASSET-incorporated iLNTB. Bar indicates 100 nm scale. Data are presented as mean ± SD, n = 12–15 per group for (b), n = 6–9 per group for (c), n = 12 per group for (d), n = 6–9 per group for (e).

showed less than 25% cell viability in all concentration range (0.125 to 1.5 μg mL^{-1}), T-iLNTB-treated cancer cells showed higher than 80% cell viability in the same concentrations of HO1 siRNA (Figure S2e, Supporting Information). Additionally, iLNTB treatment did not induce apoptosis in cancer cells (Figure S2f, Supporting Information). A previous study reported the mild antiproliferative effect of HO1-silencing in cancer cell and this study could explain our results.[9b] Next, we analyzed the damage-associated molecular pattern (DAMP) to evaluate whether iLNTB treatment might increase Dox-induced immunogenic cell death of cancer cells.[22] Only Dox treatment induced surface calreticulin (CRT) level and increased extracellular release of ATP, HMGB1 compared to control group which indicating immunogenic cell death, and iLNC treatment in combination with Dox shows comparable effect with only Dox group. Compared to only Dox and iLNC + Dox group, iLNTB-treatment in combination with Dox increased all DAMPs (CRT, extracellular ATP, HMGB1) in both B16F10, E0771 cells (Figure 2e–g). Overall, these results demonstrate the chemoboosting effect of iLNTB in cancer cells, and consequently increases Dox-induced immunogenic cancer cell death.

2.3. In Vivo Tumor-Targeted Delivery and Dual Cell-Targeted Internalization of T-iLNTB

The expression of programmed death ligand 1 (PD-L1) has been reported not only on cancer cells, but also on myeloid cells in the tumor microenvironment.[19,23] Therefore, an anti-PD-L1

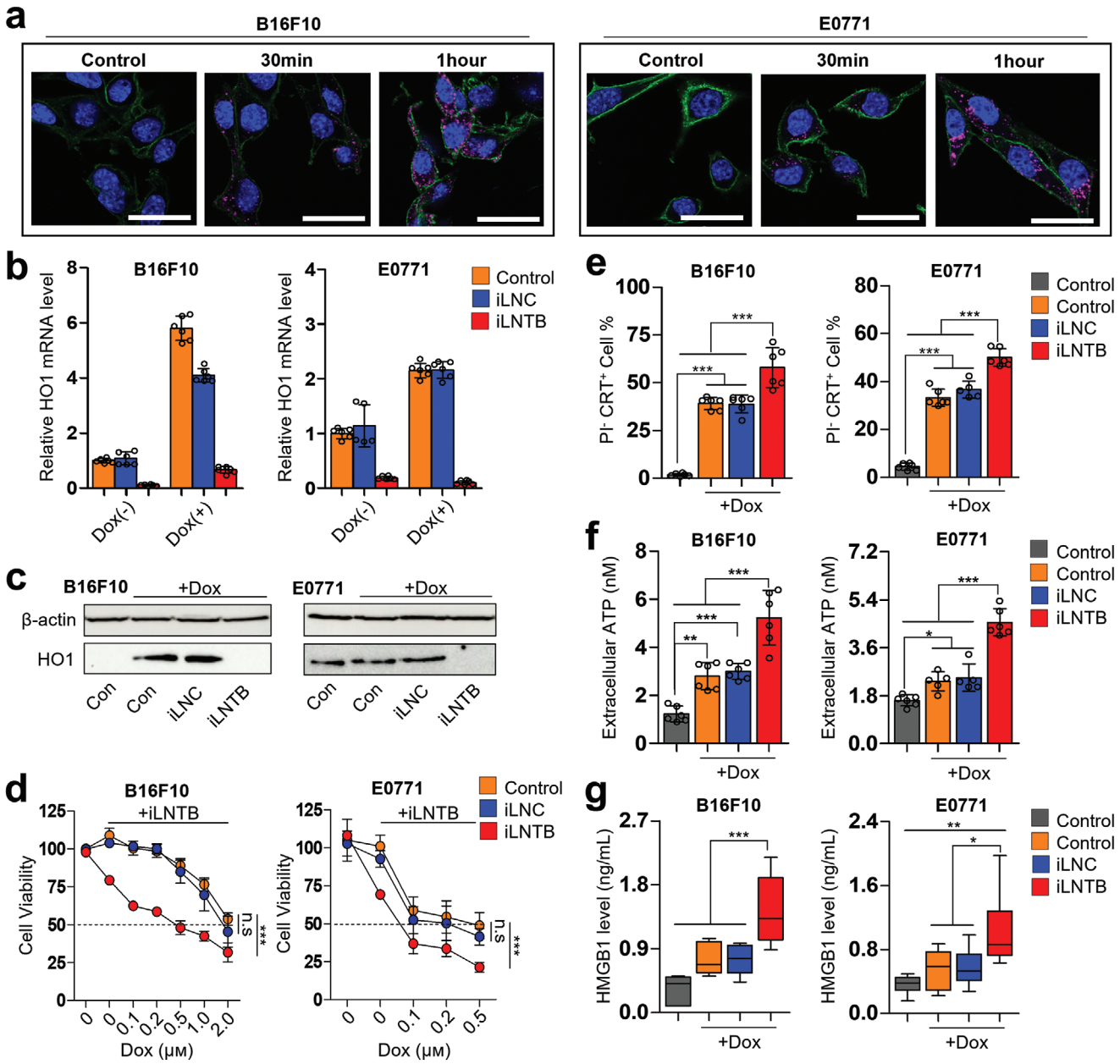

Figure 2. In vitro chemoboosting effect of iLNTB in cancer cells. a) Confocal microscopy imaging of cancer cell uptake for iLNTB. Intracellular localization of iLNTB (Cy5-siRNA) is visualized at indicated time point upon treatment of B16F10 melanoma and E0771 breast cancer cell. Magenta: siRNA, Green: CD44, cell membrane, Blue: nucleus. b) Chemoresponsive HO1 upregulation and iLNTB-mediated HO1 gene silencing in cancer cell. HO1 mRNA level was quantified by RT-PCR 72 h post iLNTB treatment. Cells were treated with Dox (1×10^{-6} M) 48 h post iLNTB treatment and incubated for additional 24 h before RNA extraction and analysis. c) Western blot image of HO1 suppression by iLNTB. d) Cell viability assay for iLNTB-mediated chemosensitization effect. Cancer cells were treated with iLNTB in combination with different concentrations of Dox, followed by cell viability assessment. ***$P < 0.001$ by two-way ANOVA with Bonferroni's post hoc test, n.s. = not significant compared to control group. e–g) iLNTB-mediated increase of Dox-induced immunogenic cell death. Cells were treated with iLNTB in combination with Dox (1×10^{-6} M) and (e) surface calreticulin (CRT) expression was analyzed in propidium iodide negative cells (PI^- cells) by flow cytometry. (f) extracellular ATP and (g) HMGB1 levels were measured in cell culture medium. Data are presented as mean ± SD ($n = 6$ per group for (b), $n = 4$–8 per group for (d), $n = 5$–6 per group for (e) and (f)). Data are presented as Box & Whiskers for (g) ($n = 7$–8 per group). *$P < 0.05$, ***$P < 0.001$ by one-way ANOVA with Tukey's post hoc test, n.s. = not significant.

antibody was employed for cancer- and tumor myeloid-dual cell-targeted delivery of iLNTB (**Figure 3**a). First, PD-L1 expression on tumor cells was analyzed in vivo, in a B16F10-bearing tumor model. Tumor myeloid cells were gated based on their expression of CD11b, Ly6C, Ly6G, and F4/80, and T cells were gated by the expression of CD3, CD8, and CD4 (Figure S3a, Supporting Information). Cells that were negative for CD31 and CD45 expression were gated as B16F10 cancer cells. B16F10 cancer

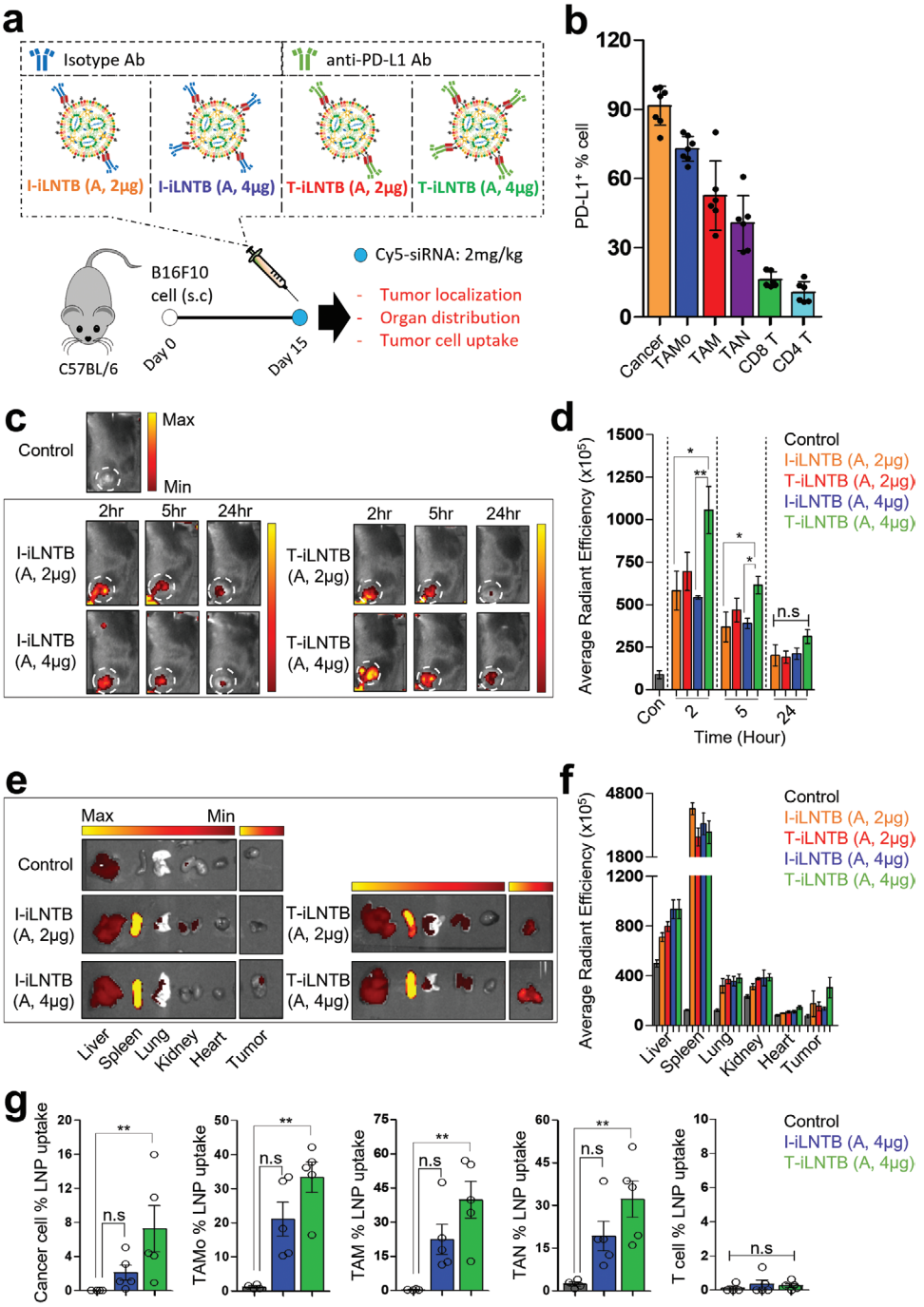

Figure 3. In vivo tumor-targeted delivery and tumor cell uptake study in murine melanoma model. a) Experimental scheme for in vivo tumor-targeted biodistribution study. B16F10 cells were subcutaneously injected to C57BL/6 mice and tumor-targeted delivery experiments were performed 15 days post cell injection. b) Bar graph for PD-L1-expression in tumor cells. Data is presented as mean ± SD, $n = 6–7$ mice. c) Representative whole-body images of in vivo tumor-targeting effect of T-iLNTB. Fluorescence intensity of Cy5-labeled siRNA in the tumor was quantified at 2, 5, and 24 h post intravenous injection of PD-L1 Ab-modified iLNTB (T-iLNTB) and isotype Ab-modified iLNTB (I-iLNTB). "A, 2 μg" and "A, 4 μg" indicate 2 μg and 4 μg of ASSET incorporation for iLNTB, respectively. d) Bar graph for average radiant efficiency of tumor-localized iLNTB in (c). Data are presented as mean ± S.E.M., $^*P < 0.05$, $^{**}P < 0.01$ by one-way ANOVA with Tukey's post hoc test, n.s. = not significant, $n = 4–5$ mice per group. e) Representative organ images for biodistribution study of iLNTB. Organs were harvested from mice 24 h post injection of T-iLNTB and I-iLNTB. f) Bar graph for average radiant efficiency in organs. g) Tumor cell uptake of T-iLNTB, analyzed by flow cytometry. Tumor cells were digested to achieve a single-cell suspension and analyzed for T-iLNTB uptake at 2 h post intravenous injection. Data are presented as mean ± S.E.M., $^{**}P < 0.01$ by nonparametric Kruskal Wallis-test, n.s. = not significant, $n = 4–5$ mice per group.

cells showed the highest PD-L1 expression with 91.5% of cells followed by tumor-associated monocytes (TAMo, 72.8%), TAM (52.5%), tumor-associated neutrophils (TAN, 40.6%), and tumor T cells that showed lower than 20% expression of PD-L1 (Figure 3b). To evaluate tumor-targeted delivery, ASSET 2 μg- and ASSET 4 μg-incorporated iLNTBs were modified with

anti-PD-L1 antibody (PD-L1 Ab) or isotype antibody (IsoAb) at a 1:2 weight ratio of ASSET to antibody and were injected intravenously into B16F10 tumor-bearing mice (Figure 3a). In Table S1 of the Supporting Information, all IsoAb- and PD-L1 Ab-modified iLNTBs show 1–2.5 nm increase of size in comparison with only ASSET-incorporated iLNTBs. Moreover, IsoAb- and PD-L1 Ab-modified iLNTBs show slight increase of ζ-potential depending on the amounts of antibodies. Anti-PD-L1-modified iLNTB (T-iLNTB, ASSET 4 μg) showed higher tumor localization than other treatment at 2, 5, and 24 h post injection (Figure 3c,d). At 2 h post injection, IsoAb-modified iLNTBs (I-iLNTB, 2 and 4 μg ASSET) showed 6.52- and 6.08-fold higher average radiant efficiency in tumor region compared to noninjected control, which is attributable to the passive tumor-targeted delivery of LNP system. Moreover, the average radiant efficiency of anti-PD-L1 modified iLNTB (T-iLNTB, ASSET 4 μg) in the tumor region at 2 h post injection was 11.85-, 1.81-, and 1.94-fold higher than noninjected control, I-iLNTB (ASSET 2 μg) and I-iLNTB (ASSET 4 μg), respectively. However, T-iLNTB (ASSET 2 μg) showed no significant enhancement for tumor-targeting in comparison with I-iLNTBs, which could be explained by insufficient targeting effect using the 2 μg ASSET with concomitant amount of anti-PD-L1 antibody. Tumor localization of all, I- and T-iLNTB was the highest at 2 h post injection and decreased over time. As for organ distribution, the strongest fluorescence signal was observed in the spleen, followed by the liver, which is the major clearance organ for LNPs. These results are in agreement with our previous studies that demonstrated a high accumulation of lipid 8-LNPs in the spleen compared to other organs, in healthy mice (Figure 3e,f).[17] Next, the tumor myeloid- and cancer-cell-targeted uptake of T-iLNTB was analyzed by flow cytometry at 2 h post injection. Anti-PD-L1-modified iLNTB (T-iLNTB, ASSET 4 μg) were taken up by 7.2%, 33.3%, 39.7%, and 32.1% of cancer cells, TAMo, TAM, and TAN, respectively. This was compared to 2.1%, 21%, 22.3%, and 19.2% of internalization for IsoAb-modified iLNTB (I-iLNTB, ASSET 4 μg) (Figure 3g; Figure S3b, Supporting information), demonstrating the highest increase (3.45-fold) for cancer cell uptake by the targeted delivery in comparison with the 1.58- to 1.78-fold increase for tumor myeloid cells uptake. However, cellular uptake rate for cancer cells is still lower than that of tumor myeloid cells which can be explained by limited ability of LNPs to penetrate the tumor efficiently. Also, the phagocytic character of myeloid cells can explain the basal uptake of I-iLNTB in tumor myeloid cells. Many of the tumor myeloid cells are recruited and distributed in perivasculature, and thus can easily meet the nanoparticles in tumor vessels (which were not analyzed here).[24] Tumor T cells did not show any uptake of T-iLNTB or I-iLNTB. On the high deviation in cellular uptake study, heterogeneity and variability of tumor microenvironment structure has led to higher deviation on the level of cellular uptake than on the level of tumor tissue accumulation. In addition, variable cellular density of the tumors (although tumors in a narrow range of size were used) could drive to the high deviation of cellular uptake. In conclusion, PD-L1 Ab-modified iLNTB (T-iLNTB) increased tumor-targeted delivery and cellular uptake of iLNTB for tumor myeloid- and cancer cells in comparison with I-iLNTB.

2.4. Antitumor and Immune Reprogramming Effect of iLNTB in combination with "Standard-of-Care" Chemotherapy

The ASSET 4 μg-incorporated iLNTB were employed in an in vivo therapeutic study based on our results from tumor targeted delivery study (Figure 3). In a previous study, human AML-bearing immunodeficient mice were used for "proof-of-concept" of HO1-targeted nanotherapeutics.[12] However, T cell deficiency in NSG mice hampers the ability to evaluate cytotoxic T cell-mediated immunotherapeutic effect, which is a major cellular compartment of the antitumor immune response. Herein, we used B16F10 melanoma-bearing mice, which represents solid tumor and metastatic stage of cancer depends on the route of administration. Moreover, melanoma is known for its immune suppression by the tumor myeloid cells infiltration.[2b] To this end, B16F10 syngeneic melanoma model was used to study the therapeutic effect of our approach and to prove the hypothesis of "Nanotherapeutic Boost" for chemo-immunotherapy. Mice were injected with iLNTB (siRNA, 2 mg kg^{-1}) twice a week combined with Dox (2.5 mg kg^{-1}, accumulative dose 7.5 mg kg^{-1} for 2 weeks) (**Figure 4**a). Combination therapy of iLNTB and Dox significantly suppressed B16F10 tumor growth compared to other treated groups (Figure 4b). T-iLNTB together with Dox showed higher antitumor effect than I-iLNTB combined with Dox, with a decrease of 0.56-fold tumor size, attributed to the tumor-targeted delivery (Figure S4a–c, Supporting Information). Prolonged median survival of 30.5 days for T-iLNTB in combination with Dox was observed compared to 22, 24, 25, and 23.5 days for PBS, Dox, T-iLNC + Dox, and T-iLNTB groups, respectively (Figure 4c). The combination therapy of iLNTB with Dox at the indicated doses did not significantly alter the body weight of the mice during the treatment, which was monitored as a general indicator for treatment toxicity (Figure S4d, Supporting Information). To evaluate the immune reprogramming effect of iLNTB, tumor immune cells were analyzed by flow cytometry (Figure 4d–i). All iLNTB treatment reduced $CD11b^+$ myeloid cell population in total tumor cells from 16.8% in PBS group to 5.4%, 8.1%, 8.5% in T-iLNTB, I-iLNTB + Dox, T-iLNTB + Dox group, respectively (Figure 4d). Detailed analysis of tumor myeloid cells demonstrated a significant decrease of TAM ($CD11b^+$ $Ly6G^-$ $F4/80^+$ $Ly6C^{-low}$) with the highest "TAMo-to-TAM" ratio in T-iLNTB + Dox group (Figure 4e). Also, the M2-like TAMs (defined as $F4/80^+$ $CD206^{-high}$) were highly decreased in all iLNTB-treated groups (Figure S4e, Supporting Information). The ratio of matured neutrophils, defined as $CD11b^+$ $Ly6G^{-high}$ cells,[25] was highly increased in T-iLNTB combined with Dox treatment group (Figure 4f). TAM are considered the major immune-suppressive cell populations, that impedes cytotoxic T cell migration into tumor tissue.[6] TAM-exclusion following T-iLNTB combined with Dox treatment explains the increase in $CD8^+$ cytotoxic T cell population (out of $CD3^+$ total T cells) and ratio of CD8 to CD4 in T-iLNTB + Dox treated mice (Figure 4g). However, total $CD3^+$ T cell % did not show significant difference between groups (Figure S4f, Supporting Information). Regulatory T cells (Treg) are major immune suppressive cells and thus decreased number of Treg cells indicates an antitumor immune responses.[26] Treg cells (defined as $CD3^+$ $CD4^+$ $CD25^+$) were significantly decreased in all iLNTB-treated groups (Figure S4g, Supporting Information). Compared to the only Dox group, T-iLNC combined with

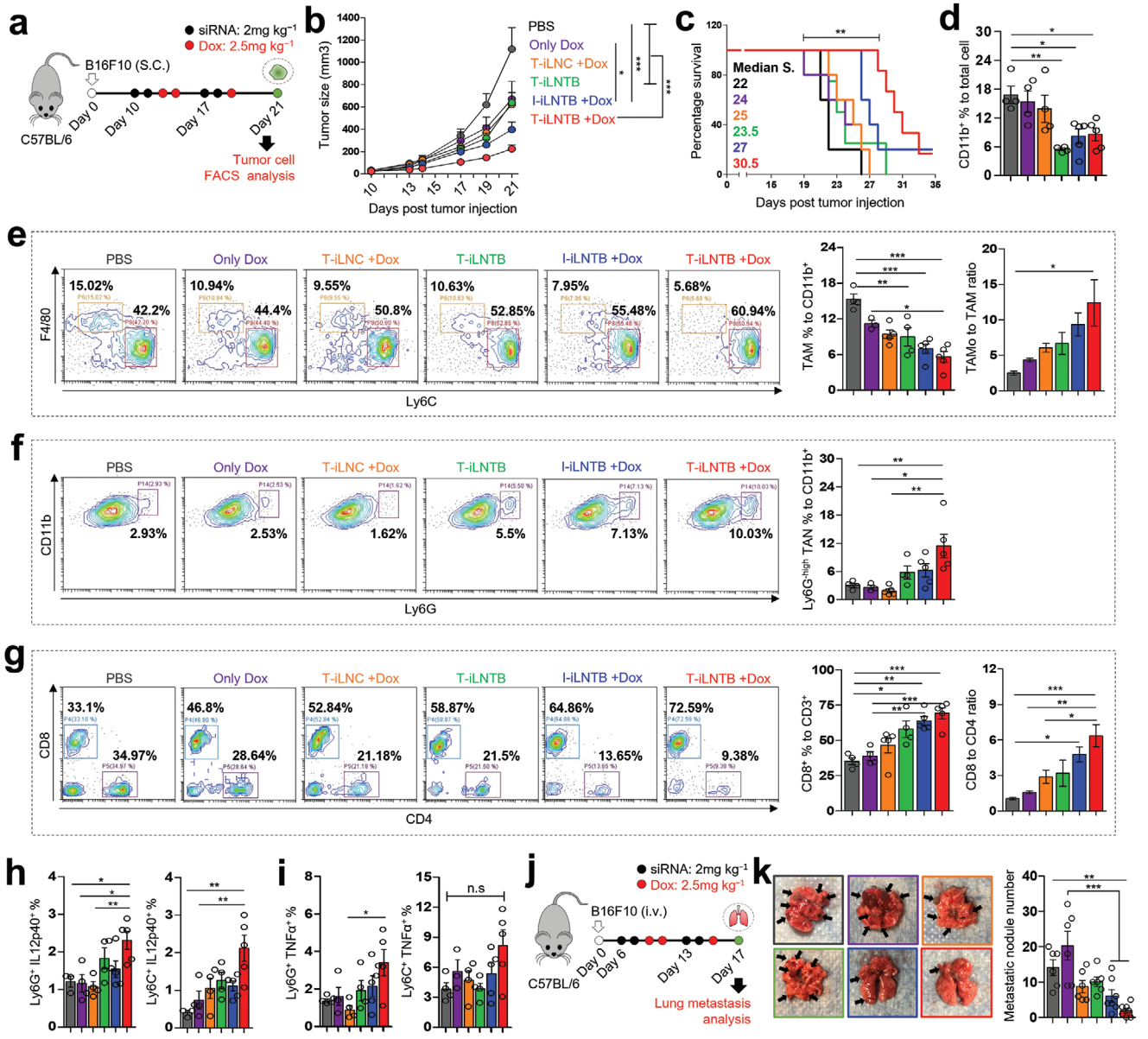

Figure 4. In vivo antitumor and immune reprogramming effect of iLNTB in combination with chemotherapy. a) Experimental scheme for in vivo therapeutic study of iLNTB. B16F10 tumor-bearing mice were treated with iLNTB (siRNA 2 mg kg^{-1}, twice a week, total 4 doses) and Dox (2.5 mg kg^{-1}, total 3 doses). b) Tumor growth curve. Size of tumor was measured at days 10, 13, 14, 17, 19, and 21 post cancer cells injection. Data presented as mean ± S.E.M., $*P < 0.05$, $**P < 0.01$, $***P < 0.001$ by two-way ANOVA with Bonferroni's post hoc test, n.s. = not significant, $n = 7$–12 mice per group. c) Survival graph. $**P < 0.01$ by log-rank (Mantel Cox) test. d) Percentile of $CD11b^+$ myeloid cells in tumor. Tumor cells were digested and analyzed by flow cytometry to quantify the ratio of $CD11b^+$ myeloid cell to total cell. e) Flow cytometry analysis of $CD11b^+$ $Ly6G^-$ tumor myeloid cells. Representative plots from each group indicate differences in TAM ($CD11b^+$ $Ly6G^-$ $F480^+$ $Ly6C^-$) and TAMo ($CD11b^+$ $Ly6G^-$ $F4/80^-$ $Ly6C^+$) populations. Percentile of TAM and TAMo-to-TAM ratio is presented. f) Flow cytometry analysis of $CD11b^+$ $Ly6G^{-high}$ tumor-associated neutrophils. g) Flow cytometry analysis of $CD4^+$ and $CD8^+$ T cells in the tumor. $CD8^+$ cytotoxic T cell ratio to $CD4^+$ helper T cell is presented. h) Intracellular IL12p40 levels in TAMo and TAN. i) Intracellular TNFα level in TAMo and TAN. Intracellular IL12p40 expression was analyzed by flow cytometry and presented as a bar graph. j) Experimental scheme for in vivo therapeutic study in a metastatic melanoma model. Mice were injected with B16F10 cells through tail vein and treated with iLNTB in combination with Dox, and lung metastasis was evaluated at day 17 post cell infusion. k) Representative lung image and bar graph of metastatic nodule count. Mice were sacrificed at day 17 post cell infusion and number of lung metastatic nodules was counted. Data are presented as mean ± S.E.M., $*P < 0.05$, $**P < 0.01$, $***P < 0.001$ by one-way ANOVA with Tukey's post hoc test, n.s. = not significant, $n = 3$–5 mice per group for (d–i), $n = 6$–7 mice per group for (k).

Dox group shows the difference only in the Treg cell ratio with a slight increase of CD8 to CD4 ratio, but no significant effects on the tumor myeloid cell parameters and tumor growth. This effect could be mediated by anti-PD-L1 Ab, the targeting ligand on the surface of T-iLNC, but did not show therapeutic benefit due to the small amount (targeting antibody dose: 10 µg per mouse). Overall, iLNTB and combination treatment reprograms tumor myeloid cells by decreasing TAMs and increasing the

ratio of TAMo and TAN cells. Also, cytotoxic T cells were highly recruited in the combination treatment groups. The exclusion of TAMs and recruitment of $CD8^+$ T cells are general features in an immunotherapeutic effect, but the function of recruited TAMo and TAN is heterogeneous. The myeloid cell-targeted immunotherapies have reported that the antitumor immune responses via the recruitment of inflammatory TAMo.[27] Also, the heterogeneity of TANs and their antitumoral function has been reported.[25a,28] The expression level of cytokines such as IL12 and TNFα was used to evaluate the inflammatory/antitumoral phenotype of the TAMo and TAN cells.[27] To this end, we characterized the antitumoral phenotype of TAMo and TAN cells by intracellular cytokine staining. Flow cytometry analysis demonstrated that the percentile of TAMo and TAN cells expressing the proinflammatory cytokines TNFα and IL12p40 are highly increased in T-iLNTB with the Dox-treated group (Figure 4h,i; Figure S5a,b, Supporting Information). This result indicates the proinflammatory and antitumoral phenotype of TAMo and TAN cells in the combination treatment. In the case of only T-iLNTB treatment, a control representing the sole effect of HO1 siRNA in target/tumor cells, the reconstitution of $CD11b^+$ tumor myeloid cells was observed. Compared to the combination treatment groups, only T-iLNTB treatment shows comparable TAM decrease (ratio to total cells), but a lower recruitment of TAMo and TAN cells which is in line with the lowest percentile of total myeloid cell and higher TAM ratio (Figure 4d,e). Also, only T-iLNTB treatment shows a modest effect on $CD8^+$ cytotoxic T cell recruitment. These observations highlight that the immunotherapeutic effect is indeed initiated by T-iLNTB-mediated reprogramming of tumor myeloid cells, but it is not sufficient to have a significant antitumor immune response alone. This could be correlated to the mild antitumor effect of only T-iLNTB group in Figure 4b. While a weak antiproliferative effect of HO1-silencing in cancer cells was observed in Figure 2d, that effect is translated to a smaller effect on tumor growth in vivo due to the limitation for tumor penetration (only less than ≈15% cellular uptake for cancer cells was shown in Figure 3g). Compared to I-iLNTB + Dox, the T-iLNTB + Dox group showed higher tumor growth inhibition effect with differences in immune cell ratios, especially for $Ly6G^{-high}$ TAN and inflammatory cytokine-expressing cells. This could be attributed to the higher cancer cell targeting effect by PD-L1 Ab (3.45-fold increased uptake for cancer cells), consequently, increased Dox-induced immunogenic cell death for the stimulation of the immune cells to exhibit a more inflammatory phenotype. In conclusion, T-iLNTB initiates immunotherapeutic effect by tumor myeloid cell reprograming with modest T cell recruitment, and Dox-induced immunogenic cancer cell death and the chemoboosting effect amplifies antitumoral immune responses via recruitment of inflammatory TAMo, TAN cells, and higher number of cytotoxic T cells, consequently demonstrates the immunologically "Cold" to "Hot" transition.[2a] Finally, tumor-targeted delivery improves the antitumoral effect of iLNTB and combination therapy.

2.5. Antitumor Effect of iLNTB in a Metastatic Melanoma Model

In advanced stages of melanoma, patients' mortality sharply increases due to metastasis of the cancer cells to other organs. Tumor myeloid cells, including TAMs, are known for their pro-metastatic role by accelerating cancer cell extravasation and pre-metastatic niche formation.[4] In a recent publication, HO1 expression level in myeloid cells showed a significant correlation with survival of metastatic cancer patients, and myeloid lineage-specific HO1-deletion attenuated metastasis of melanoma by myeloid- and lymphoid-cell reprogramming.[11d] To test the anti-metastatic effect of iLNTB and combination therapy, mice were injected with B16F10 cells through the tail vein to establish a metastatic disease, and treated with iLNTB together with Dox (Figure 4j). Combination therapy of T-iLNTB with Dox significantly decreased the number of the lung-metastatic nodule with an average count of 2 in comparison with 14.1, 20.3, 8.8, 10.1, 6.1 in PBS, Dox, T-iLNC + Dox, T-iLNTB, I-iLNTB + Dox groups, respectively (Figure 4k). Of note, Dox treated mice demonstrated a higher number of metastatic nodules than mice injected PBS (although there is no statistical significance), a phenomenon that could be explained by a previous report on chemotherapy-induced cancer metastasis.[29] Overall, combination treatment of T-iLNTB with Dox was found to have an effective anti-metastatic outcome in a melanoma model, which would have a therapeutic benefit for the treatment of advanced melanoma patients.

2.6. Triple Combination Therapy with Immune Checkpoint Inhibitor and Mechanistic Study of iLNTB-Mediated Tumor Myeloid Cell Reprogramming Effect

As previously described, combination of "standard-of-care" chemotherapy with immune checkpoint inhibitor is a commonly used regimen of chemo-immunotherapy, and most of the phase III clinical trials were reported on the Pembrolizumab, Nivolumab, and Atezolizumab.[3] Hence, we choose the anti-PD1 antibody (anti-PD1α) for triple combination therapy in our study. While the chemo-immunotherapy showed therapeutic benefits in the clinic, it still needs to be optimized in terms of the chemotherapeutic and immunotherapeutic administrations timing. The iLNTB and combination with Dox induced $CD8^+$ T cells recruitment to the tumor, which suggests that combination of iLNTB with Dox should be a pretreatment regimen for the improvement of therapeutic response to anti-PD1α therapy (Figure 4g). To this end, B16F10 tumor-bearing mice were treated with T-iLNTB in combination with Dox, followed by anti-PD1α injection to validate the nanotherapeutic boost effect for chemo-immunotherapy (**Figure 5**a). Mice body weight was monitored throughout the experiment as an indication for possible toxicity of the treatment, and was found to be consistent in all treatment groups (Figure 5b). T-iLNTB in combination with Dox treatment significantly suppressed tumor growth compared to Dox treatment at 21 days post tumor injection (Figure 5c; Figure S6a, Supporting Information). However, once iLNTB + Dox treatment is halted, the tumors show rapid growth, which is in agreement with the moderate therapeutic benefit in the survival study (Figure 4c). The addition of anti-PD1α to the T-iLNTB + Dox treatment regimen slowed the growth rate of the tumor, with 0.51-fold smaller tumor size on day 27, compared to T-iLNTB + Dox group (Figure 5c). Of note, day 19 marks the initiation of the anti-PD1α injection;

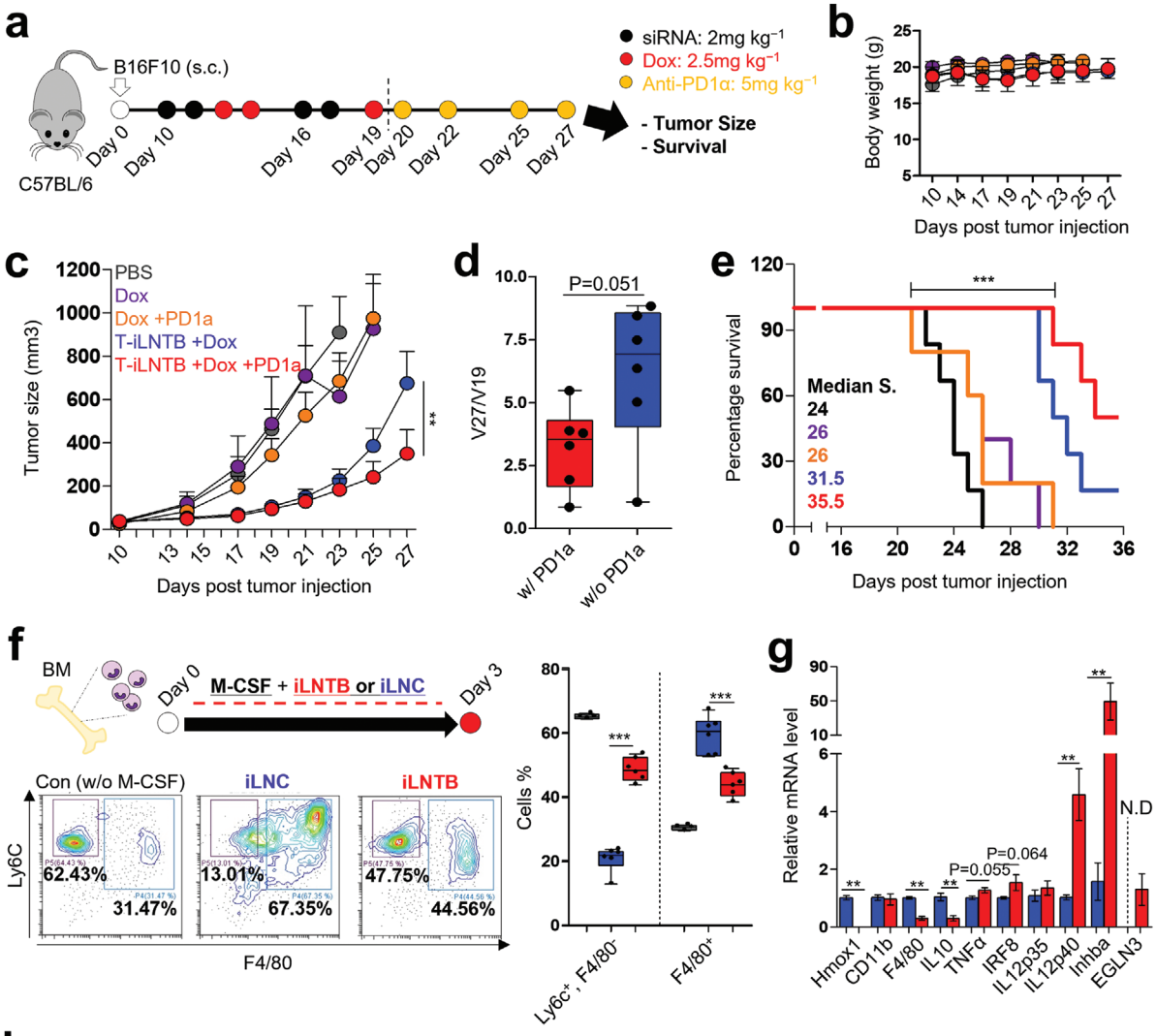

comparing the tumor volume between day 19 and day 27 highlights the effect of iLNTB on the "improved responsiveness of tumor" to anti-PD1α therapy in contrast to the nonsignificant differences observed between Dox with/without anti-PD1α therapy (Figure 5d; Figure S6b, Supporting Information). We next examined the survival of the mice treated with this triple combination. Prolonged survival for the triple combination group was observed with 50% survival rate compared to 16.6% survival for T-iLNTB + Dox group at day 36 (Figure 5e). Finally, ex vivo study was performed to understand the mechanism of iLNTB-mediated tumor myeloid reprogramming. As described in Figure 4, total myeloid cells and TAMs were significantly decreased and "TAMo-to-TAM" ratio was increased in all iLNTB-treated groups. The macrophages in the tumor vicinity mostly originate from the tumor-infiltrated monocytes, and M-CSF/CSF1R axis has been reported as a major signaling cue for TAMs differentiation/recruitment.[5a,30] To this end, the effect of iLNTB was analyzed in bone marrow cells in the presence of M-CSF which recapitulates the TAMo-to-TAM differentiation. Compared to nondifferentiated control group (without M-CSF), M-CSF treatment increased F4/80 expression on monocytic cells (from "Ly6C^{-high}, F4/80^{-}" to "Ly6C^{-high}, F4/80^{+}"), indicating macrophage differentiation. iLNTB-treated cells showed significantly different F4/80 expression, similar to nondifferentiated control group, demonstrating iLNTB-mediated inhibition of macrophage differentiation (Figure 5f). In addition, live cell gating result (FSC, SSC-based gating strategy) shows that iLNTB treatment in bone marrow cells did not induce significant cell death compared to other groups (Figure S7a, Supporting Information). This result demonstrates that the effect of HO1 siRNA in bone marrow cells is not cytotoxic, consequently, suggests noncytotoxic for the tumor myeloid cells. In Figure 5g, RT-PCR showed different proinflammatory-M1/anti-inflammatory-M2 gene expression between iLNC- and iLNTB-treated cells in the presence of M-CSF. Specifically, mRNA levels of inflammatory cytokines such as TNFα, IL12p40 was increased and the anti-inflammatory cytokine IL10 was decreased in iLNTB group compared to iLNC group. Additionally, M1-like markers inhibin A (Inhba), prolyl hydroxylase (EGLN3) and interferon regulatory factor 8 were upregulated in iLNTB group. The F4/80 mRNA levels were decreased in the iLNTB group, in line with flow cytometry results. However, the M1/M2 gene expression panel did not accurately represent the difference between inflammatory monocyte and TAM, and it should be further analyzed with a different panel of genes. Figure 5h summarizes the proposed therapeutic mechanism of T-iLNTB in combination with chemo-immunotherapy. The T-iLNTB treatment sensitizes cancer cells to conventional chemotherapy which increases chemo-induced immunogenic cell death (1) and directly reprograms tumor myeloid cells by mechanisms related to inhibition of TAM-differentiation from monocyte, as well as an increase of inflammatory TAMo and TAN cells (2). Furthermore, this approach leads to cytotoxic T lymphocytes recruitment to the tumor, which improves the therapeutic response to anti-PD1α therapy (3) and synergizes with the other indicated mechanisms for therapeutic enhancement. Lastly, we analyzed adverse effect of T-iLNTB in vivo. As we previously reported,[17] injection of lipid 8-based LNP did not induce toxic effects at 24 h post injection. Here, toxicity of T-iLNTB was evaluated at 72 h post injection to test any adverse effects induced by PD-L1-targeted LNP and HO1 gene silencing. Healthy C57Bl/6 mice were injected with 2 doses of T-iLNC or T-iLNTB and analyzed for the toxicity in major organs and blood enzymes (Figure S8a, Supporting Information). In histology images (hematoxylin and eosin staining) of major organs, no significant tissue lesions and immune cell infiltrations were observed in T-iLNTB or T-iLNC groups, compared to control (Figure S8b, Supporting Information). In addition, blood liver enzymes (SGOT, SGPT, ALP), urea, creatinine, and total protein levels did not show significant difference between the groups (Figure S8c, Supporting Information). Collectively, organ histology and liver enzyme analysis demonstrate the safety of T-iLNTB at the indicated dose. However, the maximum tolerated dose and immune-related toxicity should be addressed in our future work with experimental models, which would more accurately recapitulate human immune system, such as humanized mice-based PDX models. Ionizable lipid nanoparticle (ionizable LNP) is the most advanced nonviral nucleic acid drug delivery system, which is commercialized and clinically available for human diseases. RNA interference strategy could be an alternative due to its high target specificity, compared to small molecule inhibitors. However, tumor-targeted delivery is still a major challenge for clinical application of nanomedicine, including the use of LNPs in cancer patients. Recently, Ouyang et al. demonstrated that the number of injected nanoparticles directly influences solid tumor-targeting efficiency, the observation termed "dose threshold."[31] Specifically, it was found that a dose of more than

Figure 5. Triple combination therapy and mechanistic study of iLNTB-mediated tumor myeloid cell reprogramming effect. a) Experimental scheme of triple combination therapy. B16F10 tumor-bearing mice were treated with iLNTB and Dox for 2 weeks, followed by anti-PD1α (5 mg kg^{-1}) injection. b) Body weight monitoring throughout the experiment. c) Tumor growth curve. Size of tumor was measured at days 10, 14, 17, 19, 21, 23, 25, and 27 post cell injection. Data presented as mean ± S.E.M., $^{**}P < 0.01$ by two-way ANOVA with Bonferroni's post hoc test, n = 5–6 mice per group. d) Tumor volume ratio between day19 and day27. Data are presented as Box & Whiskers, $P = 0.051$ by Unpaired t-test, $n = 6$ mice per group. e) Survival graph. $^{***}P < 0.001$ by log-rank (Mantel Cox) test. f) Experimental scheme and flow cytometry analysis of ex vivo myeloid reprogramming. Bone marrow cells were harvested from the tibia and femur, and treated with iLNTB in presence of M-CSF (25 ng mL^{-1}) for 3 days. CD11b^{+} Ly6G^{-} F4/80^{-} Ly6C^{+} cell and CD11b^{+} Ly6G^{-} F4/80^{+} cell are defined as undifferentiated monocyte and macrophage differentiating monocyte, respectively. Data are presented as Box & Whiskers, $^{***}P < 0.001$ by one-way ANOVA with Tukey's post hoc test, n = 4–6 per group. g) RT-PCR results for inflammatory (M1)/anti-inflammatory (M2) gene expression. The mRNA levels of each gene are normalized to the mRNA levels of iLNC. N.D. (nondetectable). Data are presented as mean ± S.E.M., $^{**}P < 0.01$, $^{***}P < 0.001$ by one-way ANOVA with Tukey's post hoc test, n = 5–6 per group. h) Mechanistic summary for chemo- and immunoboosting effect of T-iLNTB. HO1-inhibiton by T-iLNTB sensitizes cancer cells to chemotherapy for enhancement of immunogenic cell death (1) and reprograms tumor myeloid cells by suppressing tumor macrophage differentiation and inducing inflammatory monocytes/neutrophils (2). Tumor myeloid cell reprogramming by iLNTB recruits CD8^{+} cytotoxic T cells to the tumor region, consequently improving the responsiveness to immune checkpoint inhibitor (3).

a trillion nanoparticles injected over the clearance capacity of Kupffer cells in the liver, with increased circulation time and improved solid tumor delivery of nanoparticles such as liposomes and gold nanoparticles. These findings have important implications on LNP and ionizable LNP for future cancer therapeutics, and a "dose threshold" study with ionizable LNPs would directly validate its potential. The immune reprogramming effect of HO1 inhibition, mainly the decreased TAMs and increased "TAMo-to-TAM" ratio, can be partially explained by the ex vivo study in bone marrow cell (Figure 5e,f). However, it is still unclear how HO1-inhibition modulates and increases $Ly6G^+$ TANs. As shown in Figure 4f; Figure S5, Supporting Information, iLNTB + Dox increased $Ly6G^{-high}$ TAN population (regarded as matured neutrophils). Previous studies reported that neutrophil function in cancer is heterogeneous, depending on the cell's maturity level.[25a] Matured neutrophils generally show higher phagocytic capacity and ROS production; Markman et al. reported an antitumoral effect of matured neutrophils in metastatic melanoma model.[28] Another limitation of our study is the apparent "mild tumor myeloid cell dependency" in our experimental models, especially regarding TAMs in the B16F10 melanoma model. In some type of human cancers, TAMs consist of up to 50% of total tumor mass, whereas in our model ~20% of $CD11b^+$ myeloid cell and lower TAM population were observed. This could be correlate to the rapid tumor growth upon termination of iLNTB + Dox treatment (Figures 4b and 5c). Overall, future studies in tumor models recapitulating human pathology such as human immune system, in patient-derived cell grafted mice would validates its therapeutic potential for human application of iLNTB. Previously, various chemo-immunotherapeutic nanoparticles were developed[7b,8] and many of them encapsulates multiple drugs such as immune activators and chemotherapeutics in one nanoparticle. However, different loading & release kinetics of the drugs, instability of nanoparticle and large-scale production method would be major obstacles for the translation of such types of nanoparticles. Phase III clinical trials and approval of the current usage of chemo-immunotherapy suggests nanotherapeutics as a separate regimen in the context of a boosting/enhancing agent for chemo-immunotherapy,[3] and this could be a more practical approach for the clinical use. Here, we applied the targeted-LNP and RNAi strategy for the therapeutic inhibition of HO1 to boost chemo-immunotherapeutic effect. Compared to other previous nanoparticles, ionizable LNP-based RNA therapeutics are highly potent for the human application which is evident by the approval of COVID19 mRNA vaccine and Patisiran. The dual-function of HO1 gene in cancer cells and tumor myeloid cells enable it as an optimal target to boost chemo-immunotherapy. In addition, RNAi-mediated HO1-inhibition overcomes current limitations of small molecule inhibitors and the ASSET system has a strong potential for tumor-targeted delivery of LNPs. Collectively, the targeted-LNP/RNAi and HO1 gene could be the best combination in the context of "nanotherapeutic boost" for chemo-immunotherapy and this could be a more practical and stronger strategy in comparison with the other previous studies. On the therapeutic potential of our system, T-iLNTB-induced therapeutic effect is derived from the two-independent mechanisms of action: the first being chemoboosting in cancer cells and the second is cancer type-independent, tumor myeloid cell reprogramming effect. To the best of our knowledge, chemoresistant function of HO1 has been reported in various type of cancer cells.[10c] Also, TAM accumulation is broadly observed feature in many types of cancers, not only in melanoma.[4] Therefore, our therapeutic strategy is most likely applicable to other type of tumor models based on its mechanisms of action.

3. Conclusions

Herein, an advanced and practical HO1-targeted nanomedicine was developed based on ionizable lipid and RNAi strategy to boost chemo-immunotherapy of cancer. Dual-cancer and -myeloid cell targeting by PD-L1 antibody increased tumor localization of iLNTB and nanotherapeutic effect. The iLNTB-mediated HO1 inhibition enhanced sensitivity to chemotherapeutics, Dox in cancer cells which increases Dox-induced immunogenic cell death (chemoboost), and reprogramed tumor myeloid cells with higher monocyte and neutrophil ratio and reduced macrophage accumulation (Immune reprogramming effect). T-iLNTB-mediated tumor myeloid reprograming and increased immunogenic cell death consequently induced infiltration of $CD8^+$ cytotoxic T cell for "Cold" to "Hot" transition in tumor microenvironment, which was correlated with improved response to anti-PD1α therapy in triple combination study (immunoboost). Intriguingly, ex vivo study in bone marrow cells proves that HO1-inhibition directly affects TAMo-to-TAM differentiation and suggests cancer type-independent myeloid cell reprogramming mechanism. In addition, iLNTB demonstrates anti-metastatic effect in advanced stage melanoma model and could be a promising therapeutic strategy in melanoma patients. Overall, dual-targeted T-iLNTB is a novel, optimal, and practical therapeutic modality for boosting the current usage of chemo-immunotherapy.

Supporting Information

Supporting Information is available from the Wiley Online Library or from the author.

Acknowledgements

The authors thank V. Holdengreber for assistance with the transmission electron microscopy analysis. This work was supported by the ERC grant LeukoTheranostics (Award No. 647410) to D.P. and the National Research Foundation of Korea, Postdoctoral Fellowship Program (2021R1A6A3A03039300) to S.-B.Y. All animal protocols were approved by the Tel Aviv University, Institutional Animal Care and Usage Committee and in accordance with current regulations and standards of the Israel Ministry of Health.

Conflict of Interest

D.P. receives licensing fees from ART Biosciences, BioNtech RNA Pharmaceuticals, Centricus, Diagnostear Ltd., EPM Inc., Earli Inc., Impetis Biosciences, Kernal Biologics, Newphase Ltd., NLC Pharma Ltd., Roche, SirTLabs Corporation, and Teva Pharmaceuticals Inc. All other authors declare no conflict of interest.

Data Availability Statement

The data that support the findings of this study are available from the corresponding author upon reasonable request.

Keywords

cancer-targeted therapy, chemo-immunotherapy, HO1-targeted nanotherapeutics, ionizable lipid nanoparticle, targeted lipid nanoparticle

Received: August 13, 2021
Revised: January 13, 2022
Published online:

[1] P. Sharma, J. P. Allison, *Science* **2015**, *348*, 56.
[2] a) M. Binnewies, E. W. Roberts, K. Kersten, V. Chan, D. F. Fearon, M. Merad, L. M. Coussens, D. I. Gabrilovich, S. Ostrand-Rosenberg, C. C. Hedrick, *Nat. Med.* **2018**, *24*, 541; b) D. Cerezo-Wallis, M. Contreras-Alcalde, K. Troulé, X. Catena, C. Mucientes, T. G. Calvo, E. Cañón, C. Tejedo, P. C. Pennacchi, S. Hogan, *Nat. Med.* **2020**, *26*, 1865.
[3] D. Salas-Benito, J. L. Pérez-Gracia, M. Ponz-Sarvisé, M. E. Rodriguez-Ruiz, I. Martínez-Forero, E. Castañón, J. M. López-Picazo, M. F. Sanmamed, I. Melero, *Cancer Discovery* **2021**, *11*, 1353.
[4] S.-B. Yong, J. Y. Chung, Y. Song, J. Kim, S. Ra, Y.-H. Kim, *Biomaterials* **2019**, *219*, 119401.
[5] a) M. Laviron, A. Boissonnas, *Front. Immunol.* **2019**, *10*, 1799; b) V. Cortez-Retamozo, M. Etzrodt, A. Newton, P. J. Rauch, A. Chudnovskiy, C. Berger, R. J. Ryan, Y. Iwamoto, B. Marinelli, R. Gorbatov, *Proc. Natl. Acad. Sci. USA* **2012**, *109*, 2491.
[6] E. Peranzoni, J. Lemoine, L. Vimeux, V. Feuillet, S. Barrin, C. Kantari-Mimoun, N. Bercovici, M. Guérin, J. Biton, H. Ouakrim, *Proc. Natl. Acad. Sci. USA* **2018**, *115*, E4041.
[7] a) T. Lang, Z. Zheng, X. Huang, Y. Liu, Y. Zhai, P. Zhang, Y. Li, Q. Yin, *Adv. Funct. Mater.* **2021**, *31*, 2007402; b) R. Yang, Z. Zhang, S. Fu, T. Hou, W. Mu, S. Liang, T. Gao, L. Guan, Y. Fang, Y. Liu, *Adv. Sci.* **2020**, *7*, 2000906.
[8] a) F. Shen, L. Feng, Y. Zhu, D. Tao, J. Xu, R. Peng, Z. Liu, *Biomaterials* **2020**, *255*, 120190; b) T. Bauleth-Ramos, M. A. Shahbazi, D. Liu, F. Fontana, A. Correia, P. Figueiredo, H. Zhang, J. P. Martins, J. T. Hirvonen, P. Granja, *Adv. Funct. Mater.* **2017**, *27*, 1703303; c) Y. He, L. Lei, J. Cao, X. Yang, S. Cai, F. Tong, D. Huang, H. Mei, K. Luo, H. Gao, *Sci. Adv.* **2021**, *7*, 0776.
[9] a) L.-Y. Chau, *J. Biomed. Sci.* **2015**, *22*, 22; b) L. Liu, Y. Wu, C. Bian, M. F. Nisar, M. Wang, X. Hu, Q. Diao, W. Nian, E. Wang, W. Xu, *Cell Commun. Signaling* **2019**, *17*, 3.
[10] a) L. Pei, Y. Kong, C. Shao, X. Yue, Z. Wang, N. Zhang, *J. Cell. Mol. Med.* **2018**, *22*, 5311; b) N. Zhe, J. Wang, S. Chen, X. Lin, Q. Chai, Y. Zhang, J. Zhao, Q. Fang, *Hematology* **2015**, *20*, 384; c) A. Furfaro, N. Traverso, C. Domenicotti, S. Piras, L. Moretta, U. Marinari, M. Pronzato, M. Nitti, *Oxid. Med. Cell. Longevity* **2016**, *2016*, 1958174.
[11] a) M. Zhang, K. Nakamura, S. Kageyama, A. O. Lawal, K. W. Gong, M. Bhetraratana, T. Fujii, D. Sulaiman, H. Hirao, S. Bolisetty, *JCI Insight* **2018**, *3*; b) T. Muliaditan, J. W. Opzoomer, J. Caron, M. Okesola, P. Kosti, S. Lall, M. Van Hemelrijck, F. Dazzi, A. Tutt, A. Grigoriadis, *Clin. Cancer Res.* **2018**, *24*, 1617; c) E. Alaluf, B. Vokaer, A. Detavernier, A. Azouz, M. Splittgerber, A. Carrette, L. Boon, F. Libert, M. Soares, A. L. Moine, *JCI Insight* **2020**, *5*; d) F. M. Consonni, A. Bleve, M. G. Totaro, M. Storto, P. Kunderfranco, A. Termanini, F. Pasqualini, C. Alì, C. Pandolfo, F. Sgambelluri, *Nat. Immunol.* **2021**, *22*, 595.
[12] S. B. Yong, J. Kim, J. Y. Chung, S. Ra, S. S. Kim, Y. H. Kim, *Adv. Sci.* **2020**, *7*, 2000487.
[13] R. Wong, H. Vreman, S. Schulz, F. Kalish, N. Pierce, D. Stevenson, *J. Perinatol.* **2011**, *31*, S35.
[14] P. La, A. P. Fernando, Z. Wang, A. Salahudeen, G. Yang, Q. Lin, C. J. Wright, P. A. Dennery, *J. Biol. Chem.* **2009**, *284*, 36302.
[15] a) A. M. Vargason, A. C. Anselmo, S. Mitragotri, *Nat. Biomed. Eng.* **2021**, *5*, 951; b) T. G. Dacoba, S. Anthiya, G. Berrecoso, I. Fernández-Mariño, C. Fernández-Varela, J. Crecente-Campo, D. Teijeiro-Osorio, F. Torres Andón, M. J. Alonso, *Adv. Funct. Mater.* **2021**, 2009860. *31*:
[16] J. Ahn, J. Ko, S. Lee, J. Yu, Y. Kim, N. L. Jeon, *Adv. Drug Delivery Rev.* **2018**, *128*, 29.
[17] S. Ramishetti, I. Hazan-Halevy, R. Palakuri, S. Chatterjee, S. Naidu Gonna, N. Dammes, I. Freilich, L. Kolik Shmuel, D. Danino, D. Peer, *Adv. Mater.* **2020**, *32*, 1906128.
[18] R. Kedmi, N. Veiga, S. Ramishetti, M. Goldsmith, D. Rosenblum, N. Dammes, I. Hazan-Halevy, L. Nahary, S. Leviatan-Ben-Arye, M. Harlev, *Nat. Nanotechnol.* **2018**, *13*, 214.
[19] P. Zhang, J. Miska, C. Lee-Chang, A. Rashidi, W. K. Panek, S. An, M. Zannikou, A. Lopez-Rosas, Y. Han, T. Xiao, *Proc. Natl. Acad. Sci. USA* **2019**, *116*, 23714.
[20] D. Rosenblum, A. Gutkin, R. Kedmi, S. Ramishetti, N. Veiga, A. M. Jacobi, M. S. Schubert, D. Friedmann-Morvinski, Z. R. Cohen, M. A. Behlke, *Sci. Adv.* **2020**, *6*, 9450.
[21] M. Obeid, A. Tesniere, F. Ghiringhelli, G. M. Fimia, L. Apetoh, J.-L. Perfettini, M. Castedo, G. Mignot, T. Panaretakis, N. Casares, *Nat. Med.* **2007**, *13*, 54.
[22] Y. Li, Y. Sun, M. Kulke, T. Hechler, K. Van der Jeught, T. Dong, B. He, K. D. Miller, M. Radovich, B. P. Schneider, *Sci. Transl. Med.* **2021**, *13*.
[23] Y. Wei, Q. Zhao, Z. Gao, X.-M. Lao, W.-M. Lin, D.-P. Chen, M. Mu, C.-X. Huang, Z.-Y. Liu, B. Li, *J. Clin. Invest.* **2019**, *129*, 3347.
[24] a) R. Hughes, B.-Z. Qian, C. Rowan, M. Muthana, I. Keklikoglou, O. C. Olson, S. Tazzyman, S. Danson, C. Addison, M. Clemons, *Cancer Res.* **2015**, *75*, 3479; b) C. E. Lewis, A. S. Harney, J. W. Pollard, *Cancer Cell* **2016**, *30*, 18.
[25] a) J. B. Mackey, S. B. Coffelt, L. M. Carlin, *Front. Immunol.* **2019**, *10*, 1912; b) J. F. Deniset, B. G. Surewaard, W.-Y. Lee, P. Kubes, *J. Exp. Med.* **2017**, *214*, 1333.
[26] R. Lima-Sousa, B. L. Melo, C. G. Alves, A. F. Moreira, A. G. Mendonça, I. J. Correia, D. de Melo-Diogo, *Adv. Funct. Mater.* **2021**, 2010777. *31*:
[27] C. J. Perry, A. R. Muñoz-Rojas, K. M. Meeth, L. N. Kellman, R. A. Amezquita, D. Thakral, V. Y. Du, J. X. Wang, W. Damsky, A. L. Kuhlmann, *J. Exp. Med.* **2018**, *215*, 877.
[28] J. L. Markman, R. A. Porritt, D. Wakita, M. E. Lane, D. Martinon, M. N. Rivas, M. Luu, E. M. Posadas, T. R. Crother, M. Arditi, *Nat. Commun.* **2020**, *11*, 1613.
[29] G. S. Karagiannis, J. M. Pastoriza, Y. Wang, A. S. Harney, D. Entenberg, J. Pignatelli, V. P. Sharma, E. A. Xue, E. Cheng, T. M. D'Alfonso, *Sci. Transl. Med.* **2017**, *9*.
[30] D. G. DeNardo, D. J. Brennan, E. Rexhepaj, B. Ruffell, S. L. Shiao, S. F. Madden, W. M. Gallagher, N. Wadhwani, S. D. Keil, S. A. Junaid, *Cancer Discovery* **2011**, *1*, 54.
[31] B. Ouyang, W. Poon, Y.-N. Zhang, Z. P. Lin, B. R. Kingston, A. J. Tavares, Y. Zhang, J. Chen, M. S. Valic, A. M. Syed, *Nat. Mater.* **2020**, *19*, 1362.